Lithos 374–375 (2020) 105723

Contents lists available at ScienceDirect

Lithos

journal homepage: www.elsevier.com/locate/lithos

Research Article

Geochemical evidences for quantifying crustal thickness over time in the Urumieh-Dokhtar magmatic arc (Iran)

Razieh Chaharlang [a], Mihai N. Ducea [b,c,*], Jalil Ghalamghash [a]

[a] Research Institute for Earth Sciences, Geological Survey of Iran, Tehran 13185-1494, Iran
[b] Department of Geosciences, University of Arizona, 1040 E. 4th Street, Tucson, AZ 85721, USA
[c] Faculty of Geology and Geophysics, University of Bucharest, 010041 Bucharest, Romania

ARTICLE INFO

Article history:
Received 21 May 2020
Received in revised form 6 August 2020
Accepted 10 August 2020
Available online 12 August 2020

Keywords:
Urumieh-Dokhtar magmatic arc
Eocene-Miocene
Crustal thickness
Collision
Neo-Tethys

ABSTRACT

Geochemical data on igneous rocks of the Urumieh-Dokhtar magmatic arc (UDMA) are used to reconstruct temporal variations in crustal thickness during the Tertiary. We use two approaches, (1) whole rock Sr/Y and La/Yb ratios, and (2) Nd isotopes and an assimilation model for magma genesis. Our results indicate that the crust was likely of normal thickness (~35 km) and remained constant during Eocene to Oligocene, corresponding to slab roll back and back arc extension along the Eurasian active margin. Crustal thickening began during the early Miocene and culminated in the middle Miocene (~50 km). This thickening is marked by a distinct increase in Sr/Y and La/Yb ratios (changing the stability of certain mineral phases) and decrease in εNd (increasing crustal assimilation). Thickening was likely due to intrusion of magma as well as crustal shortening and was a consequence of the final roll back of the Neo-Tethys slab and subsequent continental collision.

© 2020 Elsevier B.V. All rights reserved.

1. Introduction

Present day thickness of the continental crust is relatively well known at regional and global scales (Laske et al., 2013). The thickness ranges from just a few kilometers thicker than oceanic crust at island arcs to over 80 km at some convergent margins, such as in Himalaya-Tibet (Hu et al., 2017; Laske et al., 2013). Monitoring quantitative changes in crustal thickness throughout the evolution of orogenic regions has traditionally been difficult, as is the evolution of paleo-topography. Qualitatively, this has been accomplished in many regional studies aimed at deciphering timing of shortening or extension archived in the rock record. One recently applied approach to quantify past crustal thickness is the use of geochemical information from magmatic rocks as proxies for paleo-crustal thickness. Increasing crustal thickness in an arc setting can affect trace and major elemental chemistry (Chapman et al., 2015; Chiaradia, 2015; Farner and Lee, 2017; Mantle and Collins, 2008; Profeta et al., 2015) and is also typically correlated with increased crustal assimilation (Haschke et al., 2002; Scott et al., 2018), most commonly quantified via radiogenic isotopes (DePaolo, 1981).

Recently, several geochemical indicators (e.g. the ratios of Sr/Y or La/Yb and others as well as some major elements) have been used as proxies for crustal thickness in magmatic rocks (Chapman et al., 2015; Chiaradia, 2015; Farner and Lee, 2017; Mantle and Collins, 2008; Profeta et al., 2015; Turner and Langmuir, 2015). These geochemical indicators are calibrated on a regional to global scale by comparing the compositions of recently emplaced magmatic rocks to known crustal thickness from geophysical studies (see Profeta et al., 2015). Hu et al. (2017, 2020) calibrated crustal thickness to geochemical parameters for collisional orogens.

Furthermore, radiogenic isotopic results provide useful proxies for paleo-crustal thickness (Alexander et al., 2019; DePaolo et al., 2019; Turner and Langmuir, 2015) in certain orogens where the crust is isotopically distinct from the underlying mantle. This kind of study has been used in places such as the central Andes (Scott et al., 2018) where the upper plate is old and highly radiogenic. This approach has a rather limited use in places like the Coast Mountains of the Pacific NW (British Columbia and SE Alaska) where the entire upper plate is dominated by young accreted terranes that are isotopically very similar to the underlying mantle (Girardi et al., 2012). The Neodymium Crustal Index (NCI) is a good parameter to quantify crustal assimilation where appropriate. This model depends on assumed, but in places reasonably well constrained end member values of mantle and crust.

The Urumieh-Dokhtar magmatic arc (UDMA) in Iran is a part of the Zagros mountain range, which is the product of northward subduction of the Neo-Tethys followed by continental collision. The region is ideal for studying the temporal variation of crustal thickness and the effects of subduction and continental collision on crustal thickness since the upper plate is continental and relatively old. Previously, Shafiei et al.

* Corresponding author at: Department of Geosciences, University of Arizona, 1040 E. 4th Street, Tucson, AZ 85721, USA.
E-mail address: ducea@arizona.edu (M.N. Ducea).

https://doi.org/10.1016/j.lithos.2020.105723
0024-4937/© 2020 Elsevier B.V. All rights reserved.

(2009) and Asadi et al. (2014) suggested that the pre-collisional crustal thickness during Eocene-Oligocene was 30–35 km, while during the Miocene collision, the thickness increased to 45–55 km.

In this study we use trace elemental geochemistry and Nd isotopic data from previously published values on granitoids and volcanic rocks of the UDMA to investigate the systematic variations and the timing of crustal thickening and sources of magmas in the northwest part of the Zagros Orogen over the time period from 40 to 15 Ma (Eocene to middle Miocene).

2. Geological background

The NW-SE trending Zagros Orogen forms part of the Alpine-Himalayan orogenic belt and was generated as a result of the N-dipping subduction of the Neo-Tethys oceanic lithosphere, accretion and subsequent collision of the Afro-Arabia (Gondwana) plate with Central Iran from late Cretaceous to late Tertiary (e.g., Agard et al., 2011; Alavi, 1994; Berberian and King, 1981). The Zagros orogenic belt is subdivided into three parallel NW-SE trending tectonostratigraphic zones. From NW to SE the zones are the Urumieh-Dokhtar Magmatic Arc (UDMA), the Sanandaj-Sirjan Zone (SaSZ) and the Zagros Fold Belt (ZFB) (Fig. 1, Alavi, 1994).

The Urumieh-Dokhtar Magmatic Arc has a length around 1000 km and a width of 50–80 km. Subduction of the Neo-Tethys lithosphere was accompanied by the development of the UDMA, which is a continental magmatic arc (Andean type), parallel to the Zagros suture zone 150–200 km to the north (Main Zagros Thrust, Fig. 1). Magmatic activity in the UDMA started in the latest Cretaceous (Hassanzadeh and Wernicke, 2016). Verdel et al. (2011) attributed the renewed Paleogene magmatism in the UDMA to extension in response to slab roll back following a period of Cretaceous flat-slab subduction. Recent studies document the main subduction-related followed by collision-related magmatic activity throughout the Cenozoic (e.g., Babazadeh et al., 2017, 2019; Chaharlang and Ghorbani, 2020; Chiu et al., 2013; Ghalamghash et al., 2019; Ghorbani et al., 2014; Nouri et al., 2018; Sarjoughian et al., 2018a, 2018b; Sarjoughian et al., 2019; Shahsavari Alavijeh et al., 2019; Verdel et al., 2011; Yeganehfar et al., 2013).

The well-preserved latest Mesozoic-Cenozoic continental arc of Iran reveals spatial and temporal patterns of magmatism as well as across-arc geochemical variations in its evolution (Moghadam et al., 2020; Sepidbar et al., 2019). Eocene-Oligocene magmatic rocks have a geochemical signature typical of a continental arc under extension (e.g., Moghadam et al., 2020). Magmatism was active in the Eocene, with a notable magmatic flare-up that affected the UDMA from ~55 Ma until ~37 Ma (Verdel et al., 2011). A change in the nature of magmatism in the Oligocene indicates a transition from arc-like to what has been referred to as "OIB-like" geochemistry, implying a progressive increase in the involvement of an asthenosphere component, unmodified by subduction (Babazadeh et al., 2017; Verdel et al., 2011). Arc magmatism terminated with the beginning of collision during late Oligocene-Miocene (e.g., Topuz et al., 2019). According to Chiu et al. (2013), diachronous cessation of arc magmatism is consistent with an oblique collision between Arabia and Eurasia. The late Miocene-Quaternary magmatism, which has been described in the central UDMA (Babazadeh et al., 2019; Chiu et al., 2013), coincided with the onset of closure of the eastern Tethys seaway the end of Arabian underthrusting, which was also triggering the escape tectonics in Anatolia (Pang et al., 2013). Crustal thickening in Iran has been related to the oblique subduction of Neo-Tethys oceanic lithosphere beneath the region (Moghadam et al., 2016). Crustal thickness beneath the UDMA is currently ~45–55 km (Taghizadeh-Farahmand et al., 2015, Fig. 2).

3. Sample and database

We compiled literature data for thirteen regions of igneous rocks of Eocene to middle Miocene ages in the UDMA. The data include whole

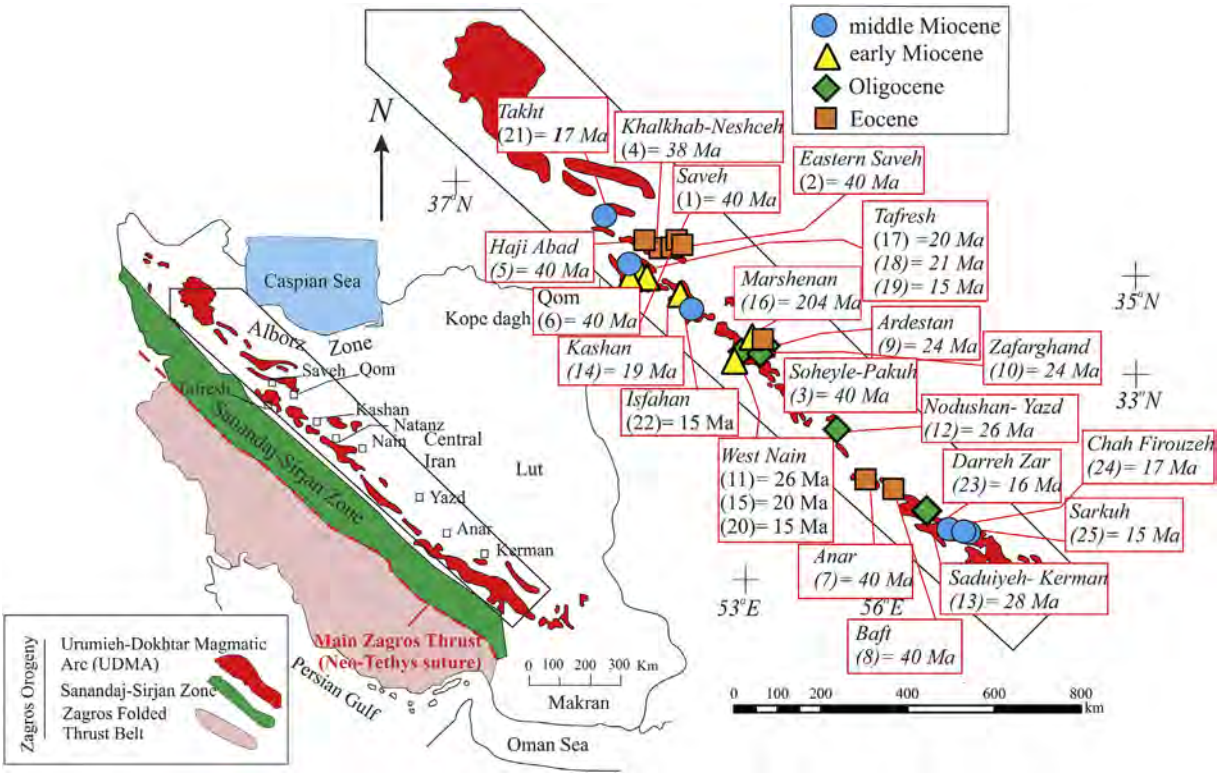

Fig. 1. The major structural units of Iran (modified after Alavi, 1994) as well as distribution of studied samples in the UDMA. source data for UDMA intrusive and volcanic ages are from Table 1.

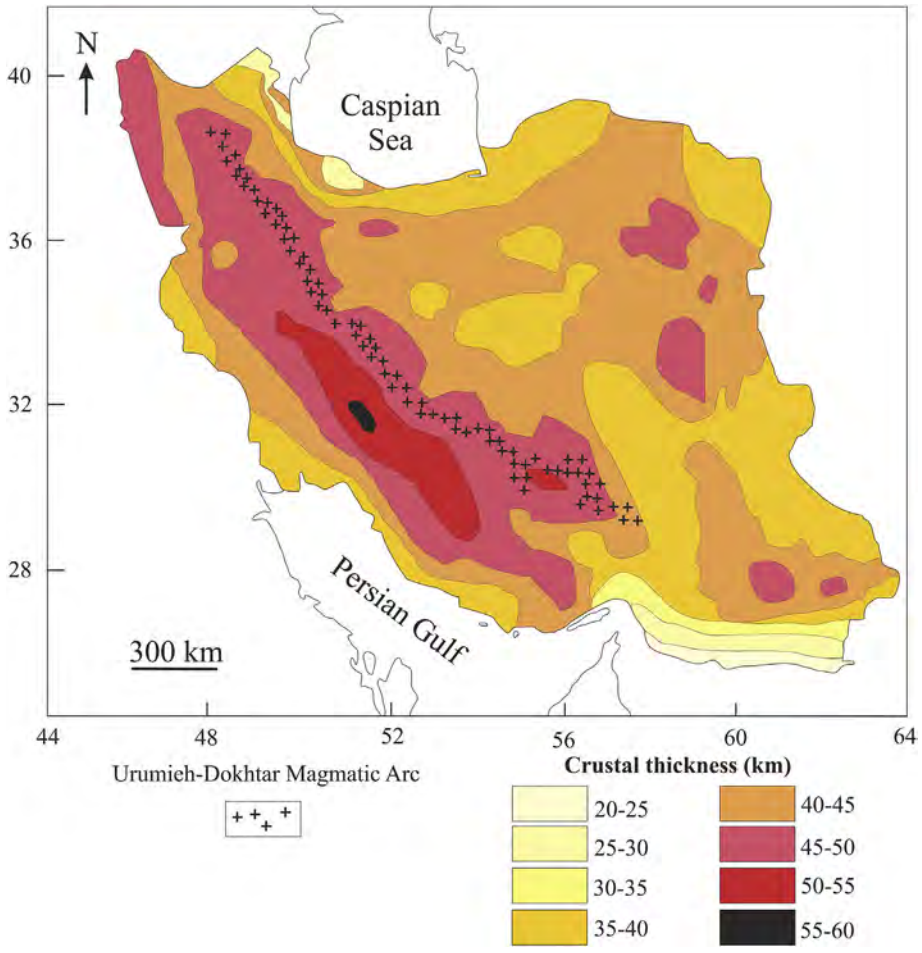

Fig. 2. Map of present day crustal thickness in Iran after Shafiei et al. (2009) and Asadi et al. (2014).

rock major and trace elemental geochemical composition (160 samples; Table 1, Table A.1). Four study areas include Eocene intrusive rocks (Saveh, Khalkhab-Neshveh, Haji Abad and Soheyle-Pakuh); another four regions consist of Oligocene intrusive rocks (Ardestan, Zafarghand, Nodushan-Yazd and Sarduiyeh); two regions are early Miocene granitoid rocks (Tafresh and Kashan) and three study areas represent middle Miocene dacitic rocks (Tafresh and Isfahan).

The data from Saveh, Khalkhab-Neshveh, Haji Abad, Soheyle-Pakuh, Ardestan, Zafarghand, Nodushan-Yazd, Sarduiyeh, west Nain, Tafresh, Marshenan, Isfahan, Takht, Darreh Zar, Chah Firouzeh and Sarkuh are also used to illustrate the isotopic composition (Nd—Sr) of igneous rocks (147 samples) from the UDMA (Table A.2). The location for the Eocene to middle Miocene samples are shown in Fig. 1 and listed Table 1.

4. Results

4.1. Major and trace elemental geochemical composition

Table A.1 lists the major and trace element data for the UDMA samples. Tertiary granitoids are gabbro, monzonite, tonalite, granodiorite and granite. Middle Miocene volcanic rocks are dacitic (Fig. 3a and b). The majority of Eocene-middle Miocene samples are calc alkaline (Peccerillo and Taylor, 1976, Fig. 3c). The Eocene-Middle Miocene granitoids and volcanic rocks in the UDMA are metaluminous to peraluminous with an alumina saturation index (ASI = molar Al_2O_3/($CaO + K_2O + Na_2O$)) of 0.7 to 1.7 (average = 0.9, Fig. 3d).

Trace elements and REEs are plotted in Fig. 4, normalized to primitive mantle (Sun and McDonough, 1989). Eocene to middle Miocene granitoids and volcanic rocks of the UDMA are enriched in large ion lithophile elements (LILEs) such as Rb, Ba, K, Pb and Sr, and depleted in high field strength elements (HFSEs) such as Nb and Ta. The middle Miocene dacitic rocks are geochemically similar to the Eocene-early Miocene granitoids except for higher contents of Th, U, Pb and Sr and lower contents of HREE (such as Lu and Yb) and Y.

Sr/Y and La/Yb ratios decrease from the Eocene to middle Miocene. Most middle Miocene dacitic rocks plot in the adakitic field in the Sr/Y vs. Y and La/Yb vs. Yb diagrams as defined by Defant and Drummond (1990) (Fig. 5). In contrast, Eocene-early Miocene granitoids typically display non adakitic Sr/Y and La/Yb ratios.

Crustal thicknesses were calculated for this study using the model of Hu et al. (2017) and are given in Table A.1. To minimize the effect of fractionation on primary magma compositions, we selected samples with a range of 55 to 72 wt% SiO_2 and MgO values 0.5 to 6 wt%. Also data were restricted to rocks with Rb/Sr = 0.05–0.2. We rejected data with average Rb/Sr > 0.35 similar to the ranges used by Hu et al. (2017).

4.2. Sr—Nd isotopes

The Sr and Nd isotope ratios of Eocene to middle Miocene granitoids and volcanic rocks in the UDMA are listed in Table A.2. The initial ratios of $^{87}Sr/^{86}Sr_{(i)}$ in the Eocene-early Miocene granitoids vary from 0.7040 to 0.7070 and their $\varepsilon Nd_{(t)}$ vary from −1.8 to +5.5. In contrast, middle Miocene granitoids and dacitic rocks have $^{87}Sr/^{86}Sr_{(i)}$ ranging from 0.7040 to 0.7080 and lower $\varepsilon Nd_{(t)}$ values from −5.3 to +0.8 (Fig. 6).

Table 1
The compositions, ages and data sources of Eocene to middle Miocene intrusive and volcanic rocks in the UDMA.

Locality	Number	Rock types	Age	Used data	Reference
Saveh	1	Diorite-tonalite-monzodiorite	40	Geochemistry-isotope	Nouri et al. (2018)
eastern Saveh	2	Trachyte-Trachybasalt-tephriphonolite	38	Isotope	Nouri et al. (2020)
Soheyle-Pakuh	3	Diorite-tonalite-monzodiorite	40	Geochemistry-isotope	Sarjoughian et al. (2019)
Khalkhab-Neshveh	4	Granodiorite-monzogabbro	38	Geochemistry-isotope	
Haji-Abad	5	Granodiorite-diorite	40	Geochemistry-isotope	Kazemi et al. (2019)
Qom	6	Basaltic andesite	40	Isotope	Omrani et al. (2008)
Anar	7	Latite	40	Isotope	Omrani et al. (2008)
Baft	8	Basaltic andesite	40	Isotope	Omrani et al. (2008)
Ardestan	9	Tonalite-diorite-granodiorite-gabbro (minor)	24	Geochemistry-isotope	Babazadeh et al. (2017)
Zafarghand	10	Granite-gabbroicdiorite	24	Geochemistry-isotope	Sarjoughian et al. (2018a)
west Nain	11	Basaltic andesite-andesite	26	Isotope	Yeganehfar et al. (2013)
Nodushan-Yazd	12	Diorite-granodiorite	25	Geochemistry-isotope	Shahsavari Alavijeh et al. (2019)
Sarduiyeh	13	Tonalite-granodiorite	28	Geochemistry-isotope	Nazarinia et al. (2018)
Kashan	14	Tonalite-granodiorite	19	Geochemistry	Honarmand et al. (2014)
west Nain	15	Basaltic andesite-andesite	20	Isotope	Yeganehfar et al. (2013)
Marshenan	16	Diorite-granodiorite-gabbroic diorite	20	Isotope	Sarjoughian et al. (2018b)
Tafresh	17	Diorite-granodiorite	20	Geochemistry	Mirnejad et al. (2019)
Tafresh	18	Diorite-granodiorite	21	Geochemistry	Raeisi et al. (2019)
Tafresh	19	Dacite	15	Geochemisrty	
west Nain	20	Dacite	15	Geochemistry	Ghorbani et al. (2014)
Takht	21	Granodiorite	17	Isotope	Haghighi Bardineh et al. (2018)
Isfahan	22	Dacite	15	Geochemistry-isotope	Khodami et al. (2009) Khodami (2019)
Darreh Zar	23	Granodiorite	16	Isotope	Asadi (2018)
Chah Firouzeh	24	Quartz-diorite	17	Isotope	Asadi (2018)
Sarkuh	25	Granodiorite	15	Isotope	Asadi (2018)

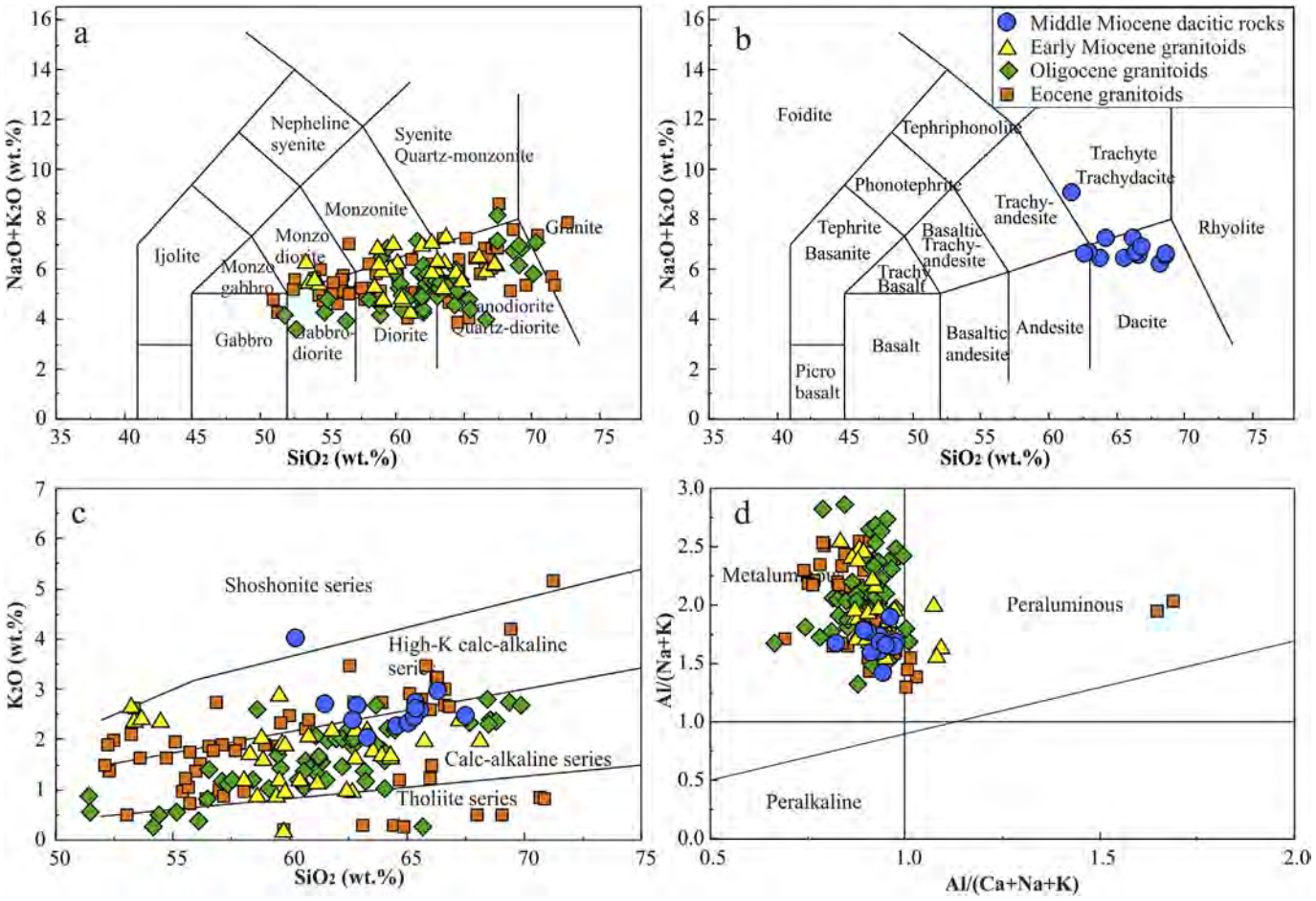

Fig. 3. $Na_2O + K_2O$ vs SiO_2 discrimination diagrams for the classification of plutonic (a) and volcanic (b) rocks from the UDMA (Middlemost, 1984). (c) K_2O vs SiO_2 diagram showing that mainly Eocene-middle Miocene rocks plot as calc alkaline to high-k calc alkaline series. (d) Al/(Na + K) vs Al/(Ca + Na + K) diagram showing the samples plot in the Metaluminous (major) to peraluminous (minor) field.

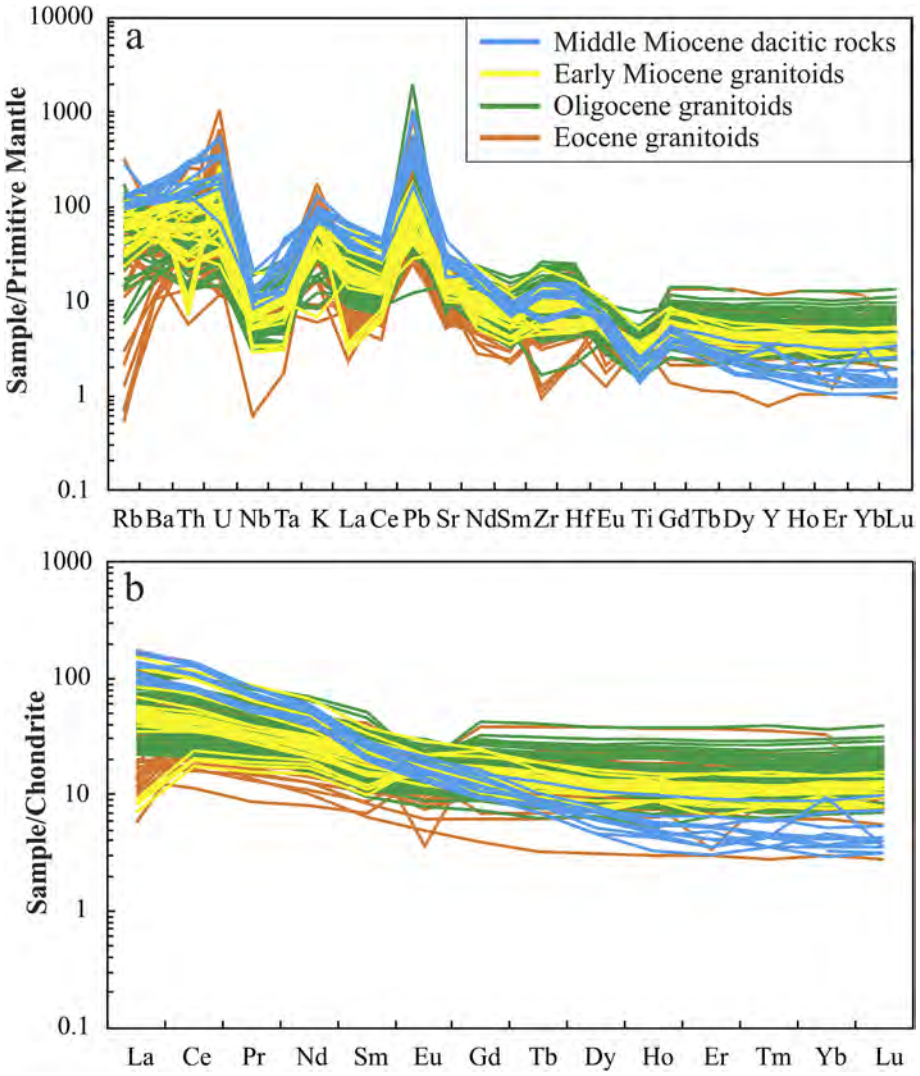

Fig. 4. (a) Trace element normalized to primitive mantle and (b) Chondrite normalized REE patterns (Sun and McDonough, 1989) for Eocene to middle Miocene plutonic and volcanic rocks from the UDMA.

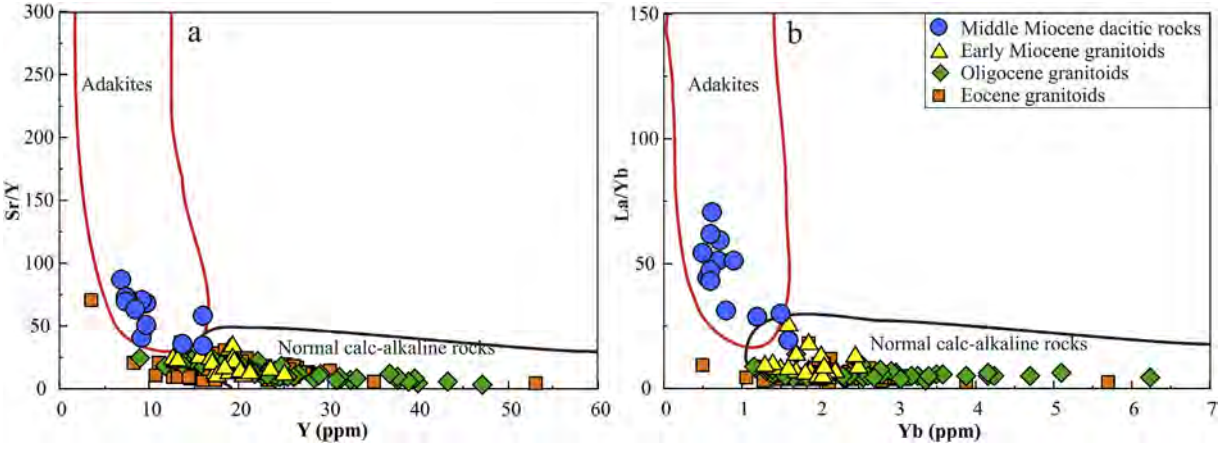

Fig. 5. (a) Sr/Y vs Y and (b) La/Yb vs Yb diagrams for Eocene to middle Miocene plutonic and volcanic rocks from the UDMA (Defant and Drummond, 1990). The middle Miocene dacitic rocks plot in the adakitic field.

5. Discussion

5.1. The nature of magmatism in the UDMA

Arc-related signatures for the UDMA intrusions and volcanic rocks include depletion in Nb—Ta and enrichment in LILE and LREE (Pearce and Peate, 1995). Moreover, the UDMA granitoids and volcanic rocks plot in the fields of volcanic arc to *syn*-collision (Pearce et al., 1984, Fig. 7a). The contribution of subduction components to the genesis of UDMA intrusive and volcanic magmas is inferred from their high Th/Yb ratios (Fig. 7b). The role of continental crustal assimilation on the UDMA igneous rocks is clear in a Th/Yb vs. SiO_2 plot (Fig. 7c). In this diagram, the more fractionated samples with higher SiO_2 contents are characterized by higher Th/Yb ratios.

The Sr isotopic compositions of the Eocene to middle Miocene igneous rocks in the UDMA show similar $^{87}Sr/^{86}Sr$ values (0.7050–0.7070), while the $\varepsilon Nd_{(t)}$ values decrease from Eocene-Oligocene to middle Miocene and is lower yet in the middle Miocene granitoids and volcanic rocks relative to Eocene-early Miocene rocks (Fig. 6). The Eocene-middle Miocene magmatic rocks plot between depleted mantle and the well characterized Iranian continental crust whose basement is Cadomian in age (Fig. 6a). The variation of εNd during Eocene to middle Miocene mostly indicates the involvement of an older continental crust or contamination by subduction-related fluids and/or melt (Haschke et al., 2010; Peate et al., 2008). Crustal contamination with late Proterozoic (Cadomian) crust is indicated by abundant inherited zircons in the Tertiary igneous rocks of the UDMA (e.g., Babazadeh et al., 2019; Chaharlang and Ghorbani, 2020; Rabiee et al., 2019).

Sr—Nd isotopes exhibit a trend consistent with mixing of mantle derived melts with assimilated crustal material, so commonly determined in arc settings globally (Ducea et al., 2015). Assuming reasonable end-member isotopic compositions, we show that granitoids and volcanic rocks from the UDMA are produced by mixing of mantle melt with 60–70% continental crust, with greater influence of pre-existing crust in the middle Miocene igneous rocks (Fig. 6a).

5.2. Trace element constraints for crustal thickening

Of particular interest here is the geochemical distinction between the UDMA middle Miocene adakites (~15 Ma) and the Eocene-early Miocene (~40–20 Ma) granitoids and volcanics. Samples from the UDMA show marked increases in Sr/Y and La/Yb from the Eocene and into the Miocene (Fig. 8). This indicates that the crust was thickening during this period. All of the Eocene to early Miocene magmatic rocks have high Y and HREE and low Sr/Y (< 40) and La/Yb (⟨20) ratios, indicating that garnet and other HREE-bearing minerals (e.g., amphibole) were absent from source rock from the granitoids and volcanic rocks were derived. Partial melting of basaltic amphibolites at intermediate pressures may produce melts in equilibrium with residues containing no garnet. This is consistent with melting of the mantle wedge beneath a crust of normal thickness (35–40 km) (e.g., Moghadam et al., 2020). This is also in good agreement with geologic constrains suggesting Eocene-Oligocene continental extension in the upper plate attributed to slab rollback (e.g., Babazadeh et al., 2017; Moghadam et al., 2020; Nouri et al., 2018; Topuz et al., 2019; Verdel et al., 2011). A further evidence for late Oligocene-early Miocene extension comes from the early Miocene intrusions in the eastern Anatolia and NW Iran formed and exhumed in an extensional setting (Moghadam et al., 2016; Topuz et al., 2019). Eocene-Oligocene crustal thinning in the UDMA could also have been attributed to lithospheric drips or delamination (e.g., Pang et al., 2013).

Sr/Y remained relatively constant (i.e., ~15) from the Eocene to the Oligocene, corresponding to an average crustal thickness of ~35 km. Starting in the early Miocene, Sr/Y increased ~20 and continued to increase into the middle Miocene, reaching a maximum in the middle Miocene, corresponding to a crustal thickness of more than 50 km (Fig. 8a). We eliminated the extremely high Sr/Y > 60 data from our calculations because they may represent slab melts or other processes that are not indicative of the crustal filter put forward by the global compilation papers of Chiaradia (2015), Profeta et al. (2015), Chapman et al. (2015) or Hu et al. (2017).

Although the La/Yb ratio is less sensitive to differences in crustal thickness in the range of 25–45 km, it can clearly show when crustal thickness exceeds about 50 km (DePaolo et al., 2019). In the plot of La/Yb versus magmatic ages (Chung et al., 2009), the La/Yb ratios of the Eocene-Miocene granitoids and volcanic rocks do increase, corresponding to a thickening of the crust (Fig. 8b). Thus, a direct implication from trace elemental constraints is that crustal thickening occurred in the UDMA during Miocene, when it thickened to >50 km. Increasing crustal thickness raises the pressure during magma fractionation at the Moho and hence changes the stability of mineral phases (Chapman et al., 2015; Profeta et al., 2015). This gradual thickening was probably a consequence of long term subduction followed by continental collision.

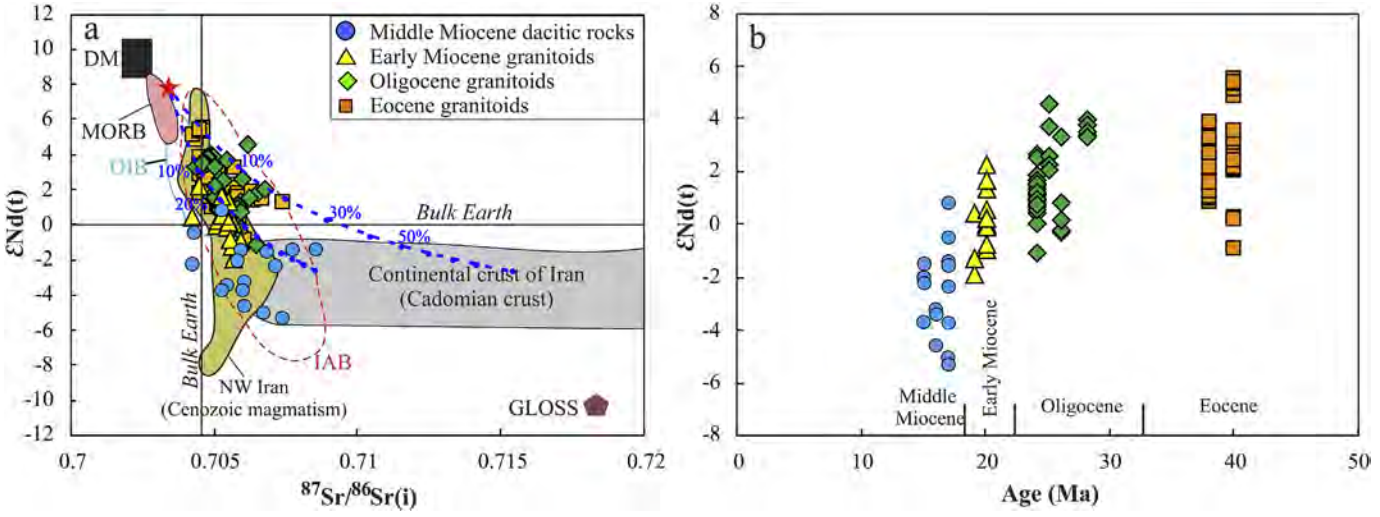

Fig. 6. $\varepsilon Nd_{(t)}$ vs (a) $^{87}Sr/^{86}Sr_{(i)}$ and (b) age (Ma) for Eocene to middle Miocene plutonic and volcanic rocks from the UDMA. The samples plot between depleted mantle and Iranian continental crust. The middle Miocene dacitic rocks show the lower $\varepsilon Nd_{(t)}$. Fields of the MORB, OIB and IAB from Vervoort et al. (1999). The composition of Cadomian continental crust is according to Moghadam et al. (2015) and Balaghi Einanlou et al. (2014) and NW Iran Cenozoic magmatism Moghadam et al. (2018).

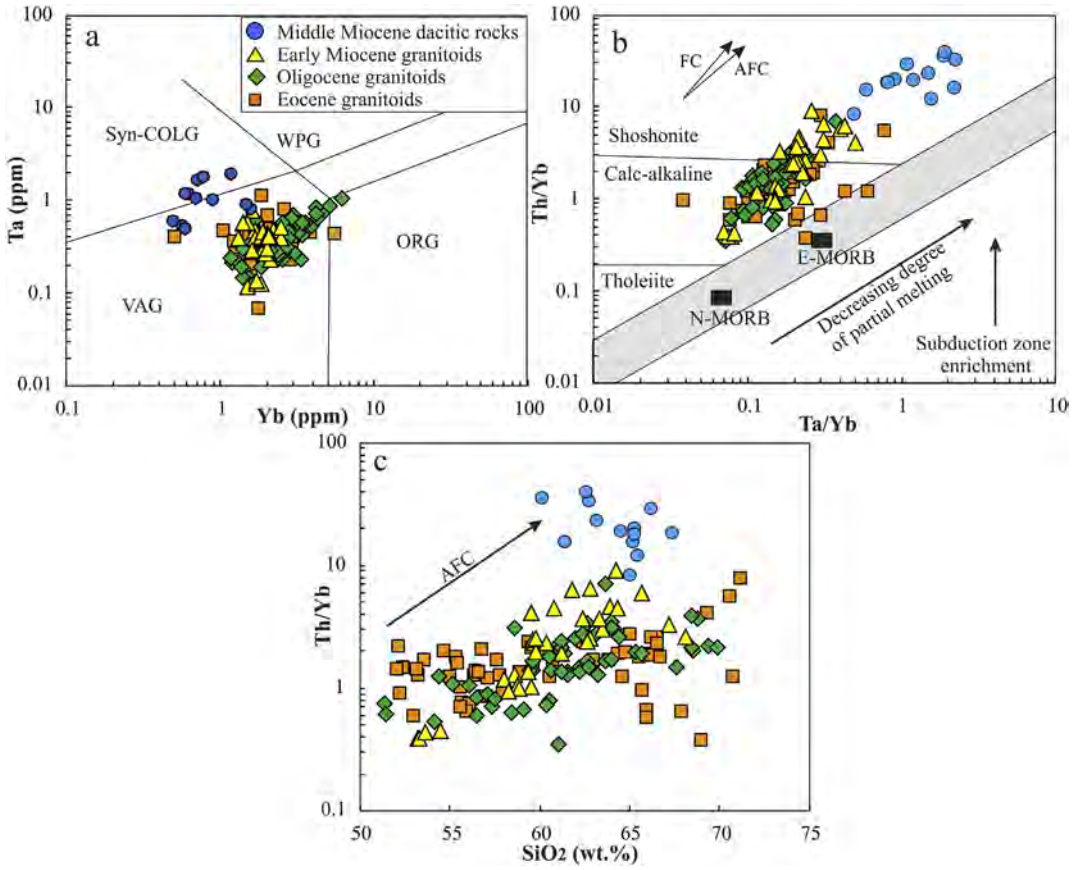

Fig. 7. (a) Tectonic discrimination diagram (Pearce, 1984). (b) Th/Yb vs Ta/Yb and (c) Th/yb vs SiO_2 diagrams for the Eocene to middle Miocene rocks from the UDMA to track the AFC processes during the genesis of these rocks.

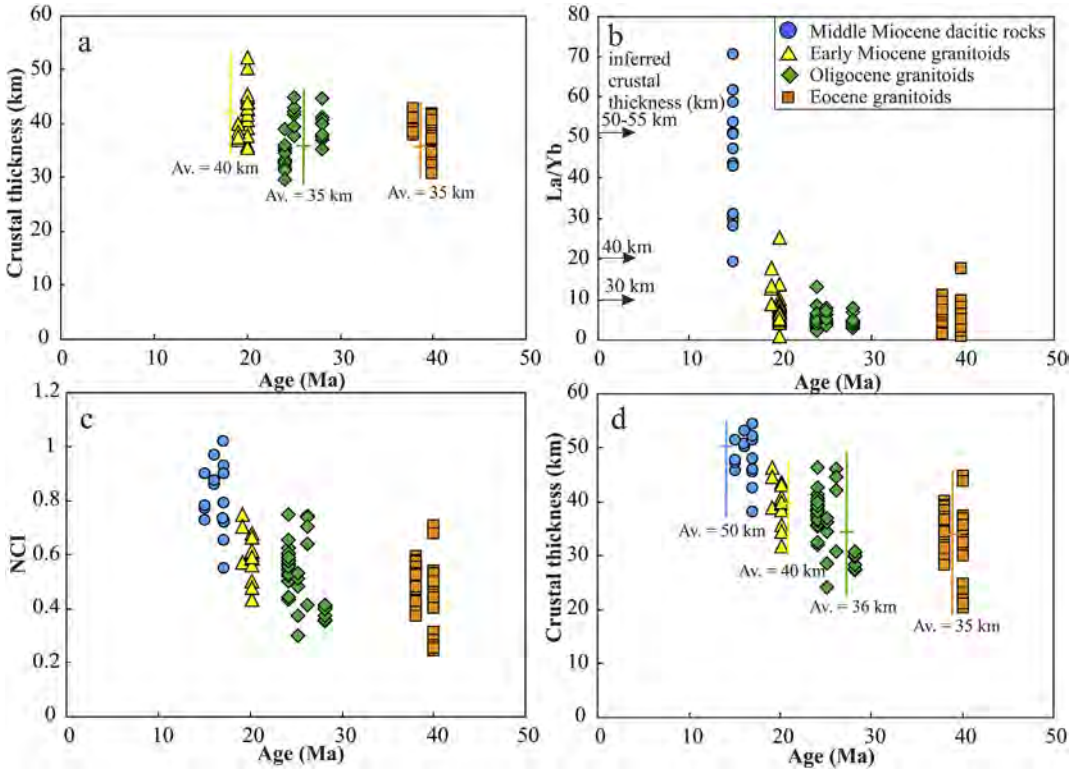

Fig. 8. Crustal thickness of the UDMA during Eocene to middle Miocene calculation by (a) Sr/Y ratios, (b) La/Yb ratios, (c) NCI ($(\varepsilon Nd - \varepsilon Nd_{(r)})/(\varepsilon Nd_{(a)} - \varepsilon Nd_{(r)})$), (d) Crustal thickness based on the whole rock εNd.

5.3. Nd Isotope constrains on crustal thickness

Sr—Nd isotopes have been used to quantify interactions between continental crustal and various mantle reservoirs (Kistler and Peterman, 1973, DePaolo, 1981 and countless papers after). Crustal materials typically contain higher $^{87}Sr/^{86}Sr$ relative to the mantle. The εNd value of continental crust is negative and decreases with increasing crustal assimilation (DePaolo et al., 1992; Peate et al., 2008). Most of the samples from the UDMA fall within a range of initial εNd of −5 to +5. Intermediate values of εNd for igneous rocks of the UDMA are here interpreted to be the result of interaction between juvenile mantle-derived melts (εNd ~ +8) and less radiogenic Cadomian continental crust of Iran (average εNd ~ −6).

Correlations between Nd isotope compositions and crustal thickness have been previously identified in areas where the upper plate is significantly older than the subducted, lower plate (e.g., Alexander et al., 2019; DePaolo et al., 2019; Scott et al., 2018). We use here the Neodymium Crustal Index (NCI) of DePaolo et al. (1992) to quantify the effect of crustal assimilation. An assumption of this model is the involvement of preexisting continental crust material (with low εNd) in the generation of magmas. This model also assumes that the εNd of mantle magma sources is relatively constant in arc settings, with values typical of the depleted mantle (DePaolo et al., 2019), which is now really constrained by data (xenoliths, basalts, etc.) in this application.

Nd isotope results and NCI calculations for Eocene to middle Miocene granitoids and volcanic rocks from the UDMA are reported in Table A.2. The NCI for these samples ranges from ~0.1 to 1 (increasing from Eocene to middle Miocene, Fig. 8c), implying variable degrees of assimilation (Fig. 8c) but increasing as a function of time. Crustal thickness beneath the UDMA range from 35 km to 50 km (Table A.2):In the Eocene-Oligocene it was thin, ~35 Km. In the middle Miocene it reached a thickness of ~50 km (Fig. 8d).

5.4. Mechanisms for crustal thickening

The trace element geochemistry and Nd isotopic data compiled here, suggest that the crust had thickened through time in the UDMA (Figs. 9, 10). La and Th contents gradually increase along with the

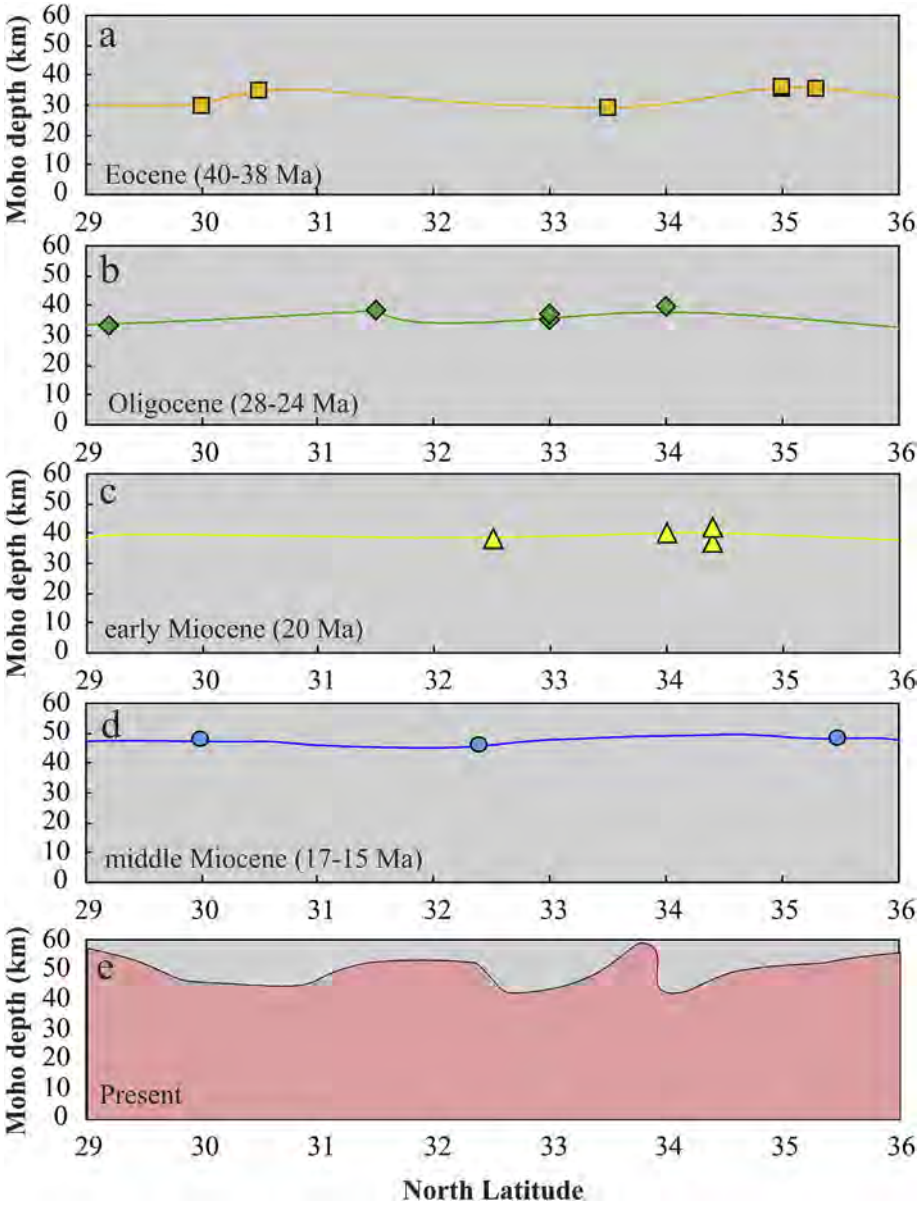

Fig. 9. Average crustal thickness over the time vs North Latitude. Average crustal thickness is calculated by using trace element ratios and whole rock εNd in the UDMA at different time periods. (a) Eocene, (b) Oligocene, (c) early Miocene, (d) middle Miocene and (e) present time.

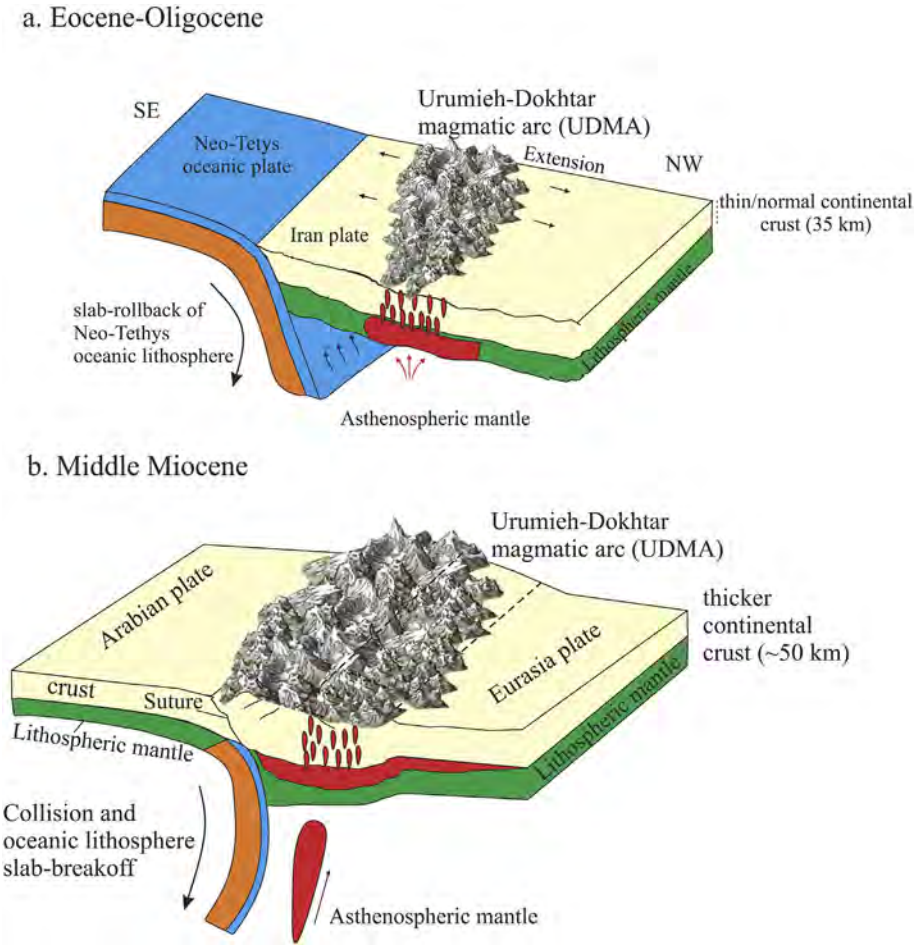

Fig. 10. Schematic diagram showing changing of crustal thickness over the time. (a) normal or thinner continental crustal thickness during Eocene-Oligocene (~35 km). (b) crustal thickening (~50 km) during middle Miocene likely due to the emplacement of magma as well as shortening (for further explanation please see the text).

decreasing Nd isotopic compositions in the middle Miocene (Fig. 11). Collisional belt rocks have higher Th and La relative to rocks from subduction arcs. One possible explanation for higher Th and La in rocks from a collisional belt, is that monazite saturation and dissolution during partial melting of the lower crust in collisional belts provides the excess Th and La (Hu et al., 2017).

The initial age of the Arabia-Eurasia collision at this location is unresolved. Proposed times for the Arabia-Eurasia collision vary from 35 to 5 Ma (e.g., Agard et al., 2011; Berberian and Berberian, 1981; Koshnaw et al., 2018; McQuarrie and van Hinsbergen, 2013; Pirouz et al., 2017; Zhang et al., 2017). However, most recent arguments suggest initial collision in late Oligocene, ca. 27 Ma (e.g., Koshnaw et al., 2018; Pirouz et al., 2017). If these recent results are correct, the crustal thickening identified here commenced after the initial collision.

Apatite (U- Th)/He cooling ages of ~20 Ma from the Saghand region of central Iran suggest an early Miocene period of north-south

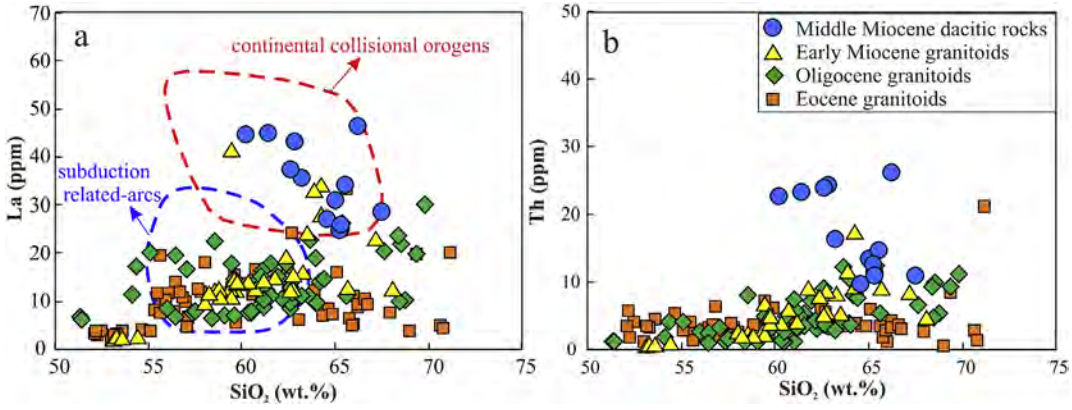

Fig. 11. Relationship whole rock La (ppm) (a), and Th (ppm) (b) vs SiO_2 (wt%) of data subsets in continental collisional belts and subduction related-arcs, reflecting uniformly high La and Th contents in the middle Miocene rocks.

shortening related to collision (Verdel et al., 2007). Approximately 200 km of shortening occurred across the Zagros and SaSZ since the onset of the collision of Eurasia-Arabia plates (Pirouz et al. (2017), of which 135 km contributed to crustal thickening of the Arabian margin and 65 km contributed to the thickening of the Eurasian margin. These results strongly suggest crustal thickening due to tectonic shortening after the collision initiation.

However, magmatic underplating may also contribute to the crustal thickening in subduction to collisional orogens (e.g., Chung et al., 2009; Ji et al., 2012; Sheffels, 1990; Zhu et al., 2017). Considering that the continental crustal thickness during subduction was 35 km, and using the exposed area for magmatic rocks, the magma production rates were ~ 200 ± 50 km^3/Myr/km during the 50–35 Ma magmatic flare-up, 15 ± 5 km^3/Myr/km for the 35–20 Ma and 30 ± 5 km^3/Myr/km for the 15–10 Ma episode (Moghadam et al., 2020). The slow and steady rate of northward subduction of Neo-Tethys oceanic plate with strongly variable rates of magma production implies magma production rates are not correlated to convergence rates (McQuarrie et al., 2003). The amount of magma addition distributed over the 35 km width of the belt could produce ~0.2 km of thickening per million years. Using these values for thickening rates during Eocene (40 Ma) to middle Miocene (15 Ma), the continental crust beneath the UDMA could have thickened by ~5 km due to magma intrusion.

6. Conclusions

Sr/Y and La/Yb ratios as well as Nd isotopic ratios for Eocene to middle Miocene igneous rocks of the UDMA reveal the following information regarding temporal variations in the crustal thickening during the Tertiary:

(1) The crust had normal thickness (~35 km) during formation of the Eocene to Oligocene magmatic rocks in the UDMA.
(2) Crustal thickening began during the early Miocene (~ 40 km) and culminated in the middle Miocene (~50 km).
(3) Crustal thickening was primarily (2/3) due to shortening but magmatic thickening also contributed an estimated 1/3 of the total.

Declaration of Competing Interest

The authors declare that they have no known competing financial interests or personal relationships that could have appeared to influence the work reported in this paper.

Acknowledgments

M.N.D. acknowledges support from US National Science Foundation grant EAR 1725002 and the Romanian Executive Agency for Higher Education, Research, Development and Innovation Funding project PN-III-P4-ID-PCCF-2016-0014. The Manuscript benefited from constructive reviews by Richard N. Abbott, Gültekin Topuz and Editor-in-Chief Xian-Hua Li.

Appendix A. Supplementary data

Supplementary data to this article can be found online at https://doi.org/10.1016/j.lithos.2020.105723.

References

Agard, P., Omrani, J., Jolivet, J., Whitechurch, H., Vrielynck, B., Spakman, W., Monié, P., Meyer, B., Wortel, R., 2011. Zagros orogeny: a subduction-dominated process. Geol. Mag. 148, 692–725.

Alavi, M., 1994. Tectonics of the Zagros orogenic belt of Iran: new data and interpretations. Tectonophysics 229, 211–238.

Alexander, E.W., Wielicki, M.M., Harrison, T.M., Depaolo, D.J., Zhao, Z.D., Zhu, D.C., 2019. Hf and Nd isotopic constraints on pre- and syn-collisional crustal thickness of southern tibet. J. Geophys. Res. Solid Earth https://doi.org/10.1029/2019JB017696.

Asadi, S., 2018. Triggers for the generation of post–collisional porphyry Cu systems in the Kerman magmatic copper belt, Iran: New constraints from elemental and isotopic (Sr–Nd–Hf–O) data. Gondwana Res. 64, 97–121.

Asadi, S., Moore, F., Zarasvandi, A., 2014. Discriminating productive and barren porphyry copper deposits in the southeastern part of the central Iranian volcano-plutonic belt, Kerman region, Iran: a review. Earth Sci. Rev. 138, 25–46.

Babazadeh, S., Ghorbani, M.R., Bröcker, M., D'Antonio, M., Cottle, J., Gebbing, T., Mazzeo, F.C., Ahmadi, P., 2017. Late Oligocene–Miocene mantle upwelling and interaction inferred from mantle signatures in gabbroic to granitic rocks from the Urumieh–Dokhtar arc, south Ardestan, Iran. Int. Geol. Rev. 59, 1590–1608. https://doi.org/10.1080/00206814.2017.1286613.

Babazadeh, S., Ghorbani, M.R., Cottle, J.M., Bröcker, M., 2019. Multistage tectono-magmatic evolution of the central Urumieh–Dokhtar magmatic arc, south Ardestan, Iran: Insights from zircon geochronology and geochemistry. Geol. J. 54, 2447–2471. https://doi.org/10.1002/gj.3306.

Berberian, F., Berberian, M., 1981. Tectono-Plutonic episodes in Iran. In: Gupta, H.K., Delany, F.M. (Eds.), American geoPhysical Union. Geodynamic Series. 3. Geological Society of America, Boulder, Colorado, pp. 5–33.

Berberian, M., King, G.C.P., 1981. Towards a paleogeography and tectonic evolution of Iran. Can. J. Earth Sci. 18, 210–265. https://doi.org/10.1139/e81-019.

Chaharlang, R., Ghorbani, M.R., 2020. A hidden crust beneath the central Urumieh-Dokhtar Magmatic Arc revealed by inherited zircon ages, Tafresh, Iran. Geol. J. 55, 3770–3781. https://doi.org/10.1002/gj.3631.

Chapman, J.B., Ducea, M.N., Profeta, L., DeCelles, P.G., 2015. Tracking changes in crustal thickness during orogenic evolution with Sr/Y; an example from the Western U.S. Cordillera. Geology 43, 919–923.

Chiaradia, M., 2015. Crustal thickness control on Sr/Y signatures of recent arc magmas: an Earth scale perspective. Sci. Rep. 5, 8115.

Chiu, H.Y., Chung, S.L., Zarrinkoub, M.H., Mohammadi, S.S., Khatib, M.M., Iizuka, Y., 2013. Zircon U–Pb age constraints from Iran on the magmatic evolution related to Neotethyan subduction and Zagros orogeny. Lithos 162–163, 70–87.

Chung, S.L., Chu, M.F., Ji, J., O'Reilly, S.Y., Pearson, N.J., Liu, D., Lee, T.Y., Lo, C.H., 2009. The nature and timing of crustal thickening in Southern Tibet: Geochemical and zircon Hf isotopic constraints from postcollisional adakites. Tectonophysics 477, 36–48.

Defant, M.J., Drummond, M.S., 1990. Derivation of some modern arc magmas by melting of young subducted lithosphere. Nature 347, 662–665.

DePaolo, D.J., 1981. Trace element and isotopic effects of combined wallrock assimilation and fractional crystallization. Earth Planet. Sci. Lett. 53, 189–202. https://doi.org/10.1016/0012-821X(81)90153-9.

DePaolo, D.J., Perry, F., Baldridge, W.S., 1992. Crustal versus mantle sources of granitic magmas: a two-parametermodel based on Nd isotopic studies. Earth Environ. Sci. Trans. R. Soc. Edinb. 83, 439–446.

DePaolo, D.J., Harrison, T.M., Wielicki, M., Zhao, Z., Zhu, D.C., Zhang, H., Mo, X., 2019. Geochemical evidence for thin syn-collision crust and major crustal thickening between 45 and 32 Ma at the southern margin of Tibet. Gondwana Res. 73, 123–135.

Ducea, M.N., Saleeby, J.B., Bergantz, G., 2015. The Architecture, Chemistry, and Evolution of Continental Magmatic Arcs. Annu. Rev. Earth Planet. Sci. 43, 10–11.

Farner, M.J., Lee, C.T., 2017. Effects of crustal thickness on magmatic differentiation in subduction zone volcanism: a global study. Earth Planet. Sci. Lett. 470, 96–107.

Ghalamghash, J., Schmitt, A.K., Chaharlang, R., 2019. Age and compositional evolution of Sahand volcano in the context of post-collisional magmatism in northwestern Iran: evidence for time-transgressive magmatism away from the collisional suture. Lithos 344-345, 265–279.

Ghorbani, M.R., Graham, L.T., Ghaderi, M., 2014. Oligocene-Miocene geodynamic evolution of the central part of Urumieh-Dokhtar Arc of Iran. Int. Geol. Rev. 56, 1039–1050.

Girardi, J.D., Patchett, P.J., Ducea, M.N., Gehrels, G.E., Robinsoncecil, M., Rusmore, M.E., Woodsworth, G.J., Pearson, D.M., Manthei, C., Wetmore, P., 2012. Elemental and isotopic evidence for granitoid Genesis from deep-seated sources in the Coast Mountains Batholith, British Columbia. J. Petrol. 53, 1505–1536.

Haghighi Bardineh, S.N., Zarei Sahamieh, R., Zamanian, H., Ahmadi Khalaji, A., 2018. Geochemical, Sr-Nd isotopic investigations and U-Pb zircon chronology of the Takht granodiorite, West Iran: evidence for postcollisional magmatism in the northern part of the Urumieh-Dokhtar magmatic assemblage. J. Afr. Earth Sci. 139, 354–366.

Haschke, M., Siebel, W., Günther, A., Scheuber, E., 2002. Repeated crustal thickening and recycling during the Andean orogeny in north Chile (21°–26°S). J. Geophys. Res. Solid Earth 107 (ECV 6–1–ECV 6–18).

Haschke, M., Ahmadian, J., Murata, M., McDonald, I., 2010. Copper mineralization prevented by arc-root delamination during Alpine-Himalayan collision in Central Iran. Econ. Geol. 105, 855–865.

Hassanzadeh, J., Wernicke, B.P., 2016. The Neotethyan Sanandaj-Sirjan zone of Iran as an archetype for passive margin-arc transitions. Tectonics 35, 586–621.

Honarmand, M., Rashidnejad Omran, N., Neubauer, F., Emami, M.H., Nabatian, G., Liu, X., Dong, X., Dong, Y., Quadt, A., Chen, B., 2014. Laser-ICP-MS U–Pb zircon ages and geochemical and Sr–Nd–Pb isotopic compositions of the Niyasar plutonic complex, Iran: constraints on petrogenesis and tectonic evolution. Int. Geol. Rev. 56, 104–132.

Hu, F., Ducea, M.N., Liu, S., Chapman, J.B., 2017. Quantifying Crustal Thickness in Continental Collisional Belts: Global Perspective and a. Geol.Appl. Nat. Sci.Rep. 7. https://doi.org/10.1038/s41598-017-07849-7.

Hu, F., Wu, F., Chapman, J.B., Ducea, M.N., Ji, W., Liu, S., 2020. Quantitatively tracking the elevation of the Tibetan Plateau sine the Cretaceous: Insights from whole-rock Sr/Y and La/Yb ratios. Geophys. Res. Lett. https://doi.org/10.1029/2020GL089202.

Ji, W.Q., Wu, F.Y., Liu, C.Z., Chung, S.L., 2012. Early Eocene crustal thickening in southern Tibet: New age and geochemical constraints from the Gangdese batholith. J. Asian Earth Sci. 53, 82–95.

Kazemi, K., Kananian, A., Xiao, Y., Sarjoughian, 2019. Petrogenesis of Middle-Eocene granitoids and their Mafic microgranular enclaves in central Urmia-Dokhtar Magmatic Arc (Iran): evidence for interaction between felsic and mafic magmas. Geosci. Front. 10, 705–723.

Khodami, M., 2019. Pb isotope geochemistry of the late Miocene–Pliocene volcanic rocks from Todeshk, the central part of the Urumieh–Dokhtar magmatic arc, Iran: Evidence of an enriched mantle source. J. Earth Syst. Sci. 128. https://doi.org/10.1007/s12040-019-1185-7.

Khodami, M., Noghreyan, M., Davoudian, A.R., 2009. Pliocene–Quaternary Adakite volcanism in the Isfahan area, Central Iranian magmatic belt. Neues Jahrbuch für Mineralogie-abhnadlungen 186, 235–248.

Kistler, R.W., Peterman, Z.E., 1973. Variations in Sr, Rb, K, Na, and initial $^{87}Sr/^{86}Sr$ in Mesozoic granitic rocks and intruded wall rocks in central California. Geol. Soc. Am. Bull. 84, 3489–3512.

Koshnaw, R.I., Stokli, D.F., Schlunegger, F., 2018. Timing of the Arabia- Eurasia continental collision—evidence from detrital zircon U-Pb geochronology of the Red Bed Series strata of the northwest Zagros hinterland, Kurdistan region of Iraq. Geology 47, 47–50.

Laske, G., Masters, G., Ma, Z., Pasyanos, M.E., 2013. Update on CRUST1.0: An updated global model of the Earth's crust. Geophys. Res. Abstr. 15. http://meetingorganizer.copernicus.org/EGU2013/EGU2013-2658.pdf.

Mantle, G.W., Collins, W.J., 2008. Quantifying crustal thickness variations in evolving orogens: Correlation between arc basalt composition and Moho depth. Geology 36, 87–90.

McQuarrie, N., van Hinsbergen, D.J.J., 2013. Retrodeforming the Arabia–Eurasia collision zone: age of collision versus magnitude of continental subduction. Geology 41, 315–318.

McQuarrie, N., Stock, M., Verdel, C., Wernicke, B.P., 2003. Cenozoic evolution of Neotethys and implications for the causes of plate motions. Geophys. Res. Lett. 30, 2036.

Mirnejad, H., Raeisi, D., McFarlane, C., Sheibi, M., 2019. Tafresh intrusive rocks within the Urumieh-Dokhtar Magmatic Arc: Appraisal of neo-tethys subduction. Geol. J. 54, 1745–1755. https://doi.org/10.1002/gj.3266.

Moghadam, H., Khademi, M., Hu, Z., Stern, R.J., Santos, J.F., Wu, Y., 2015. Cadomian (Ediacaran–Cambrian) arc magmatism in the ChahJam–Biarjmand metamorphic complex (Iran): Magmatism along the northern active margin of Gondwana. Gondwana Res. 27, 439–452. https://doi.org/10.1016/j.gr.2013.10.014.

Moghadam, H.S., Li, X.H., Stern, R.J., Ghorbani, G., Bakhshizad, F., 2016. Zircon U-Pb ages and Hf-O isotopic composition of migmatites from the Zanjan-Takab complex, NW Iran: Constraints on partial melting of metasediments. Lithos 240, 34–48.

Moghadam, H.S., Griffin, W.L., Li, X.H., Santis, J.F., Karsli, O., Stern, R.J., Ghorbani, G., Gain, S., Murphy, R., O'Reilly, S.Y., 2018. Crustal evolution of NW Iran: cadomian arcs, archean fragments and the cenozoic magmatic flare-up. J. Petrol. 58, 2143–2190.

Moghadam, H.S., Li, Q.L., Stern, R.J., Levresse, G., Santos, J.F., Lopez Martinez, M., Ducea, M.N., Ghorbani, G., Hassanzadeh, A., 2020. Neotethys subduction ignited the Iran arc and back-arc differently. J. Geophys. Res. Solid Earth https://doi.org/10.1029/2019JB018460.

Nazarinia, A., Mortazavi, M., Arvin, M., Hu, R., Zhao, C., Poosti, M., 2018. U-Pb zircon dating, Sr-Nd isotope and petrogenesis of Sarduiyeh granitoid in SE of the UDMA, Iran: implication for the source origin and magmatic Evolution. Int. Geol. Rev., 1–19 https://doi.org/10.1080/00206814.2018.1514668.

Nouri, F., Azizi, H., Stern, R.J., Asahara, Y., Khodaparast, S., Madanipour, S., Yamamoto, K., 2018. Zircon U-Pb dating, geochemistry and evolution of the late Eocene Saveh magmatic complex, Central Iran: Partial melts of sub-continental lithospheric mantle and magmatic differentiation. Lithos 314–315, 274–292.

Nouri, F., Azizi, H., Asahara, Y., Stern, R.J., 2020. A new perspective on Cenozoic calc-alkaline and shoshonitic volcanic rocks, eastern Saveh (central Iran). Int. Geol. Rev., 1–28 https://doi.org/10.1080/00206814.2020.1718005.

Omrani, J., Agard, P., Whitechurch, H., Benoit, M., 2008. Arc-magmatism and subduction history beneath the Zagros mountains, Iran: a new report of adakites and geodynamic consequences. Lithos 106, 380–398. https://doi.org/10.1016/j.lithos.2008.09.008.

Pang, K.-N., Chung, S.-L., Zarrinkoub, M.H., Khatib, M.M., Mohammadi, S.S., Chiu, H.-Y., Chu, C.-H., Lee, H.-Y., Lo, C.-H., 2013. Eocene–Oligocene post-collisional magmatism in the Lut-Sistan region, eastern Iran: magma genesis and tectonic implications. Lithos 180-181, 234–251.

Pearce, J.A., Peate, D.W., 1995. Tectonic implications of the composition of volcanic arc lavas. Annu. Rev. Earth Planet. Sci. 23, 251–285.

Pearce, J.A., Harison, N.B.W., Tindle, A.G., 1984. Trace element discrimination diagrams for the tectonic interpretation of granitic rocks. J. Petrol. 25, 956–983.

Peate, D.W., Barker, A.K., Riishuus, M.S., Andereasen, R., 2008. Temporal variations in crustal assimilation of magma suites in the East Greenland flood basalt province: Tracking the evolution of magmatic plumbing systems. Lithos 102, 179–197.

Peccerillo, A., Taylor, S.R., 1976. Geochemistry of Eocene calc-alkaline volcanic rocks from the Kastamonu area, northern Turkey. Contrib. Mineral. Petrol. 58, 63–81.

Pirouz, M., Avouac, J.P., Hassanzadeh, J., Kirschvink, J.L., Bahroudi, A., 2017. Early Neogene foreland of the Zagros, implications for the initial closure of the Neo-Tethys and kinematics of crustal shortening. Earth Planet. Sci. Lett. 477, 168–182.

Profeta, L., Ducea, M.N., Chapman, J.B., Paterson, S.R., Gonzalez, S.M.H., Kirsch, M., Petrescu, L., DeCelles, P.G., 2015. Quantifying crustal thickness over time in magmatic arcs. Sci. Rep. 5. https://doi.org/10.1038/srep17786.

Rabiee, A., Rossetti, F., Tecce, F., Asahara, Y., Azizi, H., Glodny, J., Lucci, F., Nozaem, R., Opitz, J., Selby, D., 2019. Multiphase magma intrusion, ore-enhancement and hydrothermal carbonatisation in the Siah-Kamar porphyry Mo deposit, Urumieh-Dokhtar magmatic zone, NW Iran. Ore Geol. Rev. 110, 102930.

Raeisi, D., Mirnejad, H., McFarlane, C., Sheibi, M., Babazadeh, S., 2019. Geochemistry and zircon U-Pb geochronology of Miocene plutons in the Urumieh-Dokhtar magmatic arc, East Tafresh, Central Iran. Int. Geol. Rev. https://doi.org/10.1080/00206814.2019.1600436.

Sarjoughian, F., Lentz, D., Kananian, A., Ao, S., Xiao, W., 2018a. Geochemical and isotopic constraints on the role of juvenile crust and magma mixing in the UDMA magmatism, Iran: evidence from mafic microgranular enclaves and cogenetic granitoids in the Zafarghand igneous complex. Int. J. Earth Sci. 107, 1127–1151.

Sarjoughian, F., Azizi, M., Lentz, D.R., Ling, W., 2018b. Geochemical and isotopic evidence for magma mixing/mingling in the Marshenan intrusion: Implications for juvenile crust in the Urumieh–Dokhtar Magmatic Arc, Central Iran. Geol. J. 54, 2241–2260.

Sarjoughian, F., Javadi, S., Azizi, H., Ling, W., Asahara, Y., Lentz, D., 2019. Geochemical and Sr–Nd isotopic constraints on the genesis of the Soheyle- PaKuh granitoid rocks (central Urumieh-Dokhtar magmatic belt, Iran). Int. Geol. Rev., 1–27 https://doi.org/10.1080/00206814.2019.1579676.

Scott, E.M., Allen, M.B., Macpherson, C.G., McCaffrey, K.J.W., Davidson, J.P., Saville, C., Ducea, M.N., 2018. Andean surface uplift constrained by radiogenic isotopes of arc lavas. Nat. Commun. 9 (969), 1–8. https://doi.org/10.1038/s41467-018-03173-4.

Sepidbar, F., Shafaii Moghadam, H., Zhang, L., Li, J.-W., Ma, J., Stern, R.J., Lin, C., 2019. Across-arc geochemical variations in the Paleogene magmatic belt of Iran. Lithos 344-345, 280–296.

Shafiei, B., Haschke, M., Shahabpour, J., 2009. Recycling of orogenic arc crust triggers porphyry Cu mineralization in Kerman Cenozoic arc rocks, southeastern Iran. Mineral. Deposita 44, 265–283.

Shahsavari Alavijeh, B., Rashidnejad-Omran, N., Toksoy-Köksal, Xu, W., Ghalamghash, J., 2019. Oligocene subduction-related plutonism in the Nodoushan area, Urumieh-Dokhtar magmatic belt: Petrogenetic constraints from U–Pb zircon geochronology and isotope geochemistry. Geosci. Front. 10, 725–751.

Sheffels, B.M., 1990. Lower bound on the amount of crustal shortening in the central Bolivian Andes. Geology 18, 812–815.

Sun, S.S., McDonough, W.F., 1989. Chemical and isotopic systematics of oceanic basalts: implications for mantle composition and processes. Geol. Soc. Lond. Spec. Publ. 42, 313–345.

Taghizadeh-Farahmand, F., Afshari, N., Sodoudi, F., 2015. Crustal Thickness of Iran Inferred from Converted Waves: Pure and Applied Geophysics. 172, pp. 309–331.. https://doi.org/10.1007/s00024-014-0901-0.

Topuz, G., Candan, O., Zack, T., Chen, F., Li, Q.L., 2019. Origin and significance of early Miocene high-potassium I-type granite plutonism in the East Anatolian plateau (the Tas¸lıçay intrusion). Lithos 348-348, 105210.

Turner, S.J., Langmuir, C.H., 2015. What processes control the chemical composition of arc front stratovolcanoes? Geochem. Geophys. Geosyst. 16, 1865–1893.

Verdel, C., Wernicke, B.P., Ramezani, J., Hassanzadeh, J., Renne, P.R., Spell, T.L., 2007. Geology and thermochronology of Tertiary Cordilleran-style metamorphic core complexes in the Saghand region of central Iran. Geol. Soc. Am. Bull. 119, 961–977.

Verdel, C., Wernicke, B.P., Hassanzadeh, J., Guest, B., 2011. A Paleogene extentional arc flare-up in Iran. Tectonic 30, TC3008. https://doi.org/10.1029/2010TC002809.

Vervoort, J., Patchett, P.J., Blichert-Toft, J., 1999. Relationships between Lu–Hf and Sm–Nd isotopic systems in the global sedimentary system. Earth Planet. Sci. Lett. 168, 79–99.

Yeganehfar, H., Ghorbani, M.R., Shinjo, R., Ghaderi, M., 2013. Magmatic and geodynamic evolution of Urumieh-Dokhtar basic volcanism, Central Iran: major, trace element, isotopic and geochronologic mplications. Int. Geol. Rev. 55, 767–786.

Zhang, Z., Xiao, W., Majidifard, M.R., Zhu, R., Wan, B., Ao, S., Chen, L., Rezaeian, M., Esmaeili, R., 2017. Detrital zircon provenance analysis in the Zagros Orogen, SW Iran: implications for the amalgamation history of the Neo-Tethys. Int. J. Earth Sci. 106, 1223–1238.

Zhu, D.C., Wang, Q., Cawood, P.A., Zhao, Z.D., Mo, X.X., 2017. Raising the Gangdese Mountains in southern Tibet. J. Geol. Res.Solid Earth 122, 214–223.